

## Article

# Tannic Acid/Fe<sup>III</sup> Complexes Coating PAN Nanofibrous Membrane for Highly Efficient Photocatalytic Degradation of Dyeing Wastewater

Xuefei Chen <sup>1</sup>, Lubing Zha <sup>1</sup>, Fangmeng Zeng <sup>1</sup>, Jie Meng <sup>2</sup>, Tiandi Pan <sup>1</sup> and Jindan Lv <sup>3,\*</sup>

<sup>1</sup> College of Textile Science and Engineering (International Institute of Silk), Zhejiang Sci-Tech University, Hangzhou 310018, China; chxuefei@zstu.edu.cn (X.C.); chaluu@foxmail.com (L.Z.); z\_fmeng@outlook.com (F.Z.); pantianti@zstu.edu.cn (T.P.)

<sup>2</sup> School of Engineering, Westlake University, Hangzhou 310024, China; meng\_jie\_@hotmail.com

<sup>3</sup> College of Textiles, Zhejiang Fashion Institute of Technology, Ningbo 315211, China

\* Correspondence: 17815636091@163.com

**Abstract:** Considering photocatalytic degradation technology has recently attracted great attention for dyeing wastewater treatment, the polyacrylonitrile (PAN) nanofibrous membrane coated with the TA/Fe<sup>III</sup> complexes was proposed as a novel photocatalyst in this work. The successful self-assembly of TA/Fe<sup>III</sup> complexes on the PAN nanofibrous membrane after layer-by-layer deposition of TA and Fe<sup>III</sup> was confirmed by the analyses of chemical structure, morphology, and hydrophilicity. With the number of coating cycles, more TA/Fe<sup>III</sup> complexes coated on the PAN nanofibrous membrane, which contributed to the excellent photocatalytic activity. Whereas, when the coating cycles reached seven, the photocatalytic performance of the modified PAN nanofibrous membrane deteriorated due to the serious aggregation of TA/Fe<sup>III</sup> complexes. Under optimum five coating cycles, owing to its great light absorbance capability, the modified PAN nanofibrous membrane achieved 98% degradation efficiency of RhB after 360 min illumination. This work would offer a promising high-performance photocatalyst for dyeing wastewater treatment.

**Keywords:** photocatalysis; PAN nanofibrous membrane; TA/Fe<sup>III</sup> complexes; coating cycle



**Citation:** Chen, X.; Zha, L.; Zeng, F.; Meng, J.; Pan, T.; Lv, J. Tannic Acid/Fe<sup>III</sup> Complexes Coating PAN Nanofibrous Membrane for Highly Efficient Photocatalytic Degradation of Dyeing Wastewater. *Coatings* **2023**, *13*, 1212. <https://doi.org/10.3390/coatings13071212>

Academic Editor: Peter P. Levin

Received: 9 June 2023

Revised: 28 June 2023

Accepted: 4 July 2023

Published: 6 July 2023



**Copyright:** © 2023 by the authors. Licensee MDPI, Basel, Switzerland. This article is an open access article distributed under the terms and conditions of the Creative Commons Attribution (CC BY) license (<https://creativecommons.org/licenses/by/4.0/>).

## 1. Introduction

With the rapid development of the textile industry, more and more dyeing wastewater was discharged into the environment, resulting in seriously water pollution [1]. The untreated dyes are highly harmful to living organisms even at very low concentrations (<1 ppm) [2]. Accordingly, various techniques including adsorption, coagulation, membrane filtration, and oxidation have been used to treat the dyeing wastewater [3–6]. Whereas these treatment methods are inefficient, cumbersome, and costly, that may even generate some undesirable compounds. In comparison, photocatalytic degradation is a promising alternative owing to its advantages of sustainability, energy conservation, and lack of secondary pollutants [7,8].

Common photocatalysts include inorganic metal oxides, organic semiconductors, metal-organic complexes (MOCs), and so on. Titanium dioxide (TiO<sub>2</sub>) and zinc oxide (ZnO) are the representative inorganic metal oxides widely used as photocatalysts with excellent photocatalysis. However, large bandgaps limit their optical response range to the ultraviolet region which accounts for only 5% of the solar spectrum [9,10]. Although organic semiconductors such as the graphitic carbon nitride (g-C<sub>3</sub>N<sub>4</sub>) have narrow bandgaps, rapid recombination of photogenerated electron-hole pairs greatly affects the photocatalytic efficiency [11]. Compared with inorganic and organic photocatalysts, MOCs have attracted much attention due to semiconductor-like behavior, tunable structure, and high specific surface area [12]. Nevertheless, the prevalent drawbacks of photocatalysts mentioned

above also affect the photocatalytic activity of MOCs [13]. For obtaining the broad absorption of visible light and effective separation of electron-hole pairs and transfer, doping, or loading of different catalysts are used to realize the construction of efficient MOC photocatalysts [14,15]. The complicated preparation process increases the difficulty of photocatalyst industrialization and the cost of wastewater treatment. Therefore, much effort should be made to develop new MOCs with high photocatalytic efficiency, simplified preparation, and low cost.

Tannic acid (TA), a natural plant polyphenol, can be combined with metal ions to form MOCs, for example, TA/Fe<sup>III</sup> complexes [16]. Due to the great capacity of light absorption, Cheng et al. enhanced the light harvesting of triazine-based covalent organic frameworks by incorporating TA/Fe<sup>III</sup> complexes for high photocatalytic performance [17]. Cakar et al. used the TA/Fe<sup>III</sup> complexes to broaden the spectrum response of ZnO for obtaining better photovoltaic properties in dye-sensitized solar cells [18]. Meanwhile, because of the universal adhesion property, easy synthesis, and catalytic activity, TA/Fe<sup>III</sup> complexes are widely used in the fields of electrocatalysis, photodynamic therapy, and Fenton reaction [19–21]. Nevertheless, as far as we know, there are quite a few research studies about the TA/Fe<sup>III</sup> complexes as the photocatalyst for dyeing wastewater treatment.

In this work, we report the polyacrylonitrile (PAN) nanofibrous membrane coated with the TA/Fe<sup>III</sup> complexes as a novel photocatalyst for dyeing wastewater treatment. The PAN nanofibrous membranes were fabricated by the electrospinning technology and then coated with TA/Fe<sup>III</sup> complexes through layer-by-layer deposition of TA and Fe<sup>III</sup>. The chemical structures, morphologies, and hydrophilicities of modified PAN nanofibrous membranes with different coating cycles were investigated. In particular, the capabilities of light absorbance of modified nanofibrous membranes were discussed for analyzing the mechanism of photocatalysis. Moreover, the photocatalytic activities of different modified PAN nanofibrous membranes were discussed and analyzed in detail.

## 2. Experimental

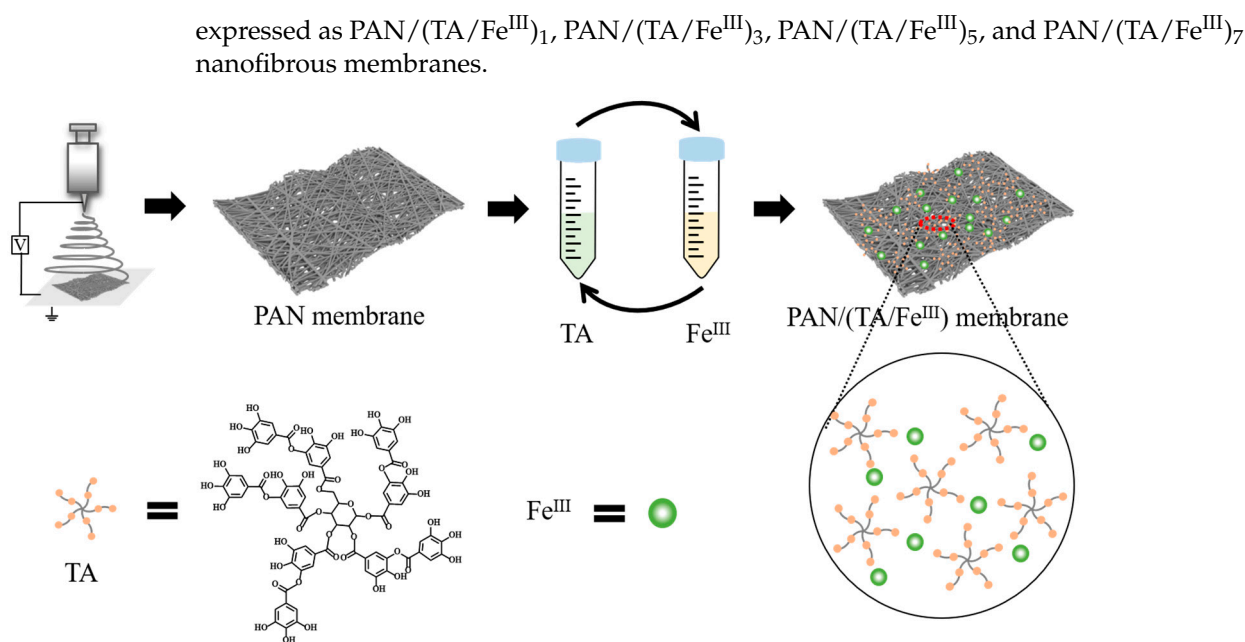
### 2.1. Materials

Polyacrylonitrile (PAN, Mw = 85,000) powders were purchased from Aladdin Chemistry Co., Ltd., Shanghai, China. N,N-dimethylformamide (DMF, 99.5%) was supplied by Shanghai Lingfeng Chemical Reagents Co., Ltd, Shanghai, China. Tannic acid (TA), FeCl<sub>3</sub>·6H<sub>2</sub>O and ethanol (99.8%) were obtained from Macklin Biochemical CO., Ltd., Shanghai, China. Rhodamine B (RhB) was supplied by Tianjin Kemiou Chemical Reagent Co., Ltd, Tianjin, China. All chemicals were used as received.

### 2.2. Preparation of PAN/(TA/Fe<sup>III</sup>) Nanofibrous Membranes

PAN solution for electrospinning was prepared by dissolving 10 wt% PAN powders in DMF and stirring at 50 °C for 6 h. The prepared PAN solution was filled into a 10 mL plastic syringe and ejected from a 20-gauge metal needle onto a silicon-coated sheet using an electrospun device (JDF05, Changsha Nanoapparatus Co., Limited, Changsha, China). The high voltage power (12 kV), the flow rate (8 uL/min), and the needle-to-collector distance (10 cm) were fixed. The PAN fibers were collected for 6 h to obtain the PAN nanofibrous membrane at 23 ± 2 °C and 35 ± 2% relative humidity.

The PAN/(TA/Fe<sup>III</sup>) nanofibrous membranes were prepared by layer-by-layer deposition of TA and Fe<sup>III</sup> according to the literature with slight modifications [22]. As shown in Scheme 1, the above PAN nanofibrous membrane (5 × 5 cm) was firstly placed in a 50 mL beaker for 10 min in which 20 mL of TA solution (3.2 mg/mL). The membrane was taken out and rinsed with ethanol for 1 min. And then the membrane was placed in a beaker of 20 mL FeCl<sub>3</sub>·6H<sub>2</sub>O solution (3.2 mg/mL) for another 10 min. Finally, the membrane was thoroughly rinsed with ethanol for 1 min. This whole treatment process was defined as one coating cycle. The coating process was repeated the preset number of coating times (1, 3, 5, and 7 times). The modified PAN nanofibrous membranes were



**Scheme 1.** Schematic illustration of preparation of PAN nanofibrous membranes coated with TA/Fe<sup>III</sup> complexes by layer-by-layer deposition.

### 2.3. Physicochemical Characterizations

The morphologies and elemental compositions of the bare PAN nanofibrous membrane and PAN/(TA/Fe<sup>III</sup>) nanofibrous membranes were investigated using a field emission scanning electron microscopy (FE-SEM, Ultra 55, ZEISS, Oberkochen, Germany) equipped with an energy dispersive X-ray spectroscopy analyzer (EDS). The fiber diameters were analyzed by ImageJ (National Institutes of Health, Bethesda, MD, USA) based on the method proposed by Hotaling et al. [23]. The chemical structures of the bare PAN nanofibrous membrane and PAN/(TA/Fe<sup>III</sup>) nanofibrous membranes were monitored over 4000–600 cm<sup>-1</sup> using a Fourier transform infrared spectroscopy (FTIR, NICOLET 5700, NICOLET, Madison, WI, USA) equipped with an ATR device with diamond plate. X-ray photoelectron spectroscopy (XPS) was measured to analyze the chemical compositions of membranes by a K-Alpha instrument (Thermo Fisher Scientific, Waltham, MA, USA). Water contact angles of the membranes were investigated using an optical contact angle instrument (DSA20, KRÜSS, Hamburg, Germany) at room temperature. Ultraviolet-visible-near-infrared diffuse reflectance spectra (UV-vis-NIR spectra) were detected on a UV-vis-NIR spectrophotometer equipped with an integrating sphere BaSO<sub>4</sub> (UH4150, Hitachi Limited, Tokyo, Japan) in wavelength range of 300–1200 nm.

### 2.4. Photocatalytic Activity Evaluation

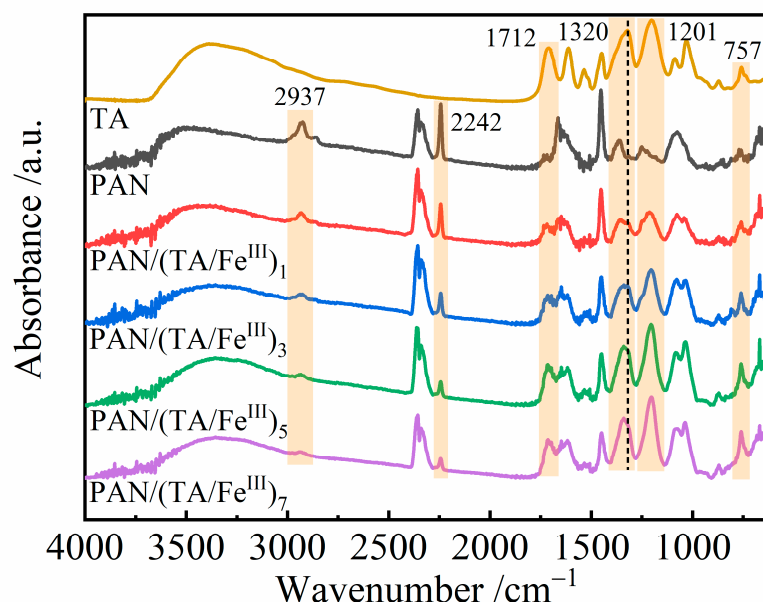
The photocatalytic activities of the membranes were evaluated based on the degradation of RhB under visible light irradiation. The visible light source was supplied by the simulated solar light of xenon lamp (300 W), which a UV cutoff filter of 420 nm was used to eliminate the UV light. The membrane (25 mg) was immersed into the 20 mL of RhB solution (10 mg/L) for 60 min in a dark environment to reach the adsorption-desorption equilibrium and then was placed under the visible light for the photocatalytic experiment. According to the Beer–Lambert law (Supplementary Figure S1), the concentration of RhB solution at the given intervals was analyzed by the absorption intensity of 554 nm in the UV-vis spectrum (UV1102, Prism Instrument, Shanghai, China). The RhB degradation rate (%) was calculated after 360 min illumination based on the equation: Degradation (%) = (C<sub>0</sub> – C)/C<sub>0</sub> × 100%, where C<sub>0</sub> and C are the initial and actual concentrations of RhB, respectively. The stability of the photocatalyst was evaluated by comparing

the degradation efficiency after the successive photocatalysis cycle. Each photocatalysis cycle was set to 360 min.

### 3. Results and Discussion

#### 3.1. Preparation and Characterizations of PAN/(TA/Fe<sup>III</sup>) Nanofibrous Membranes

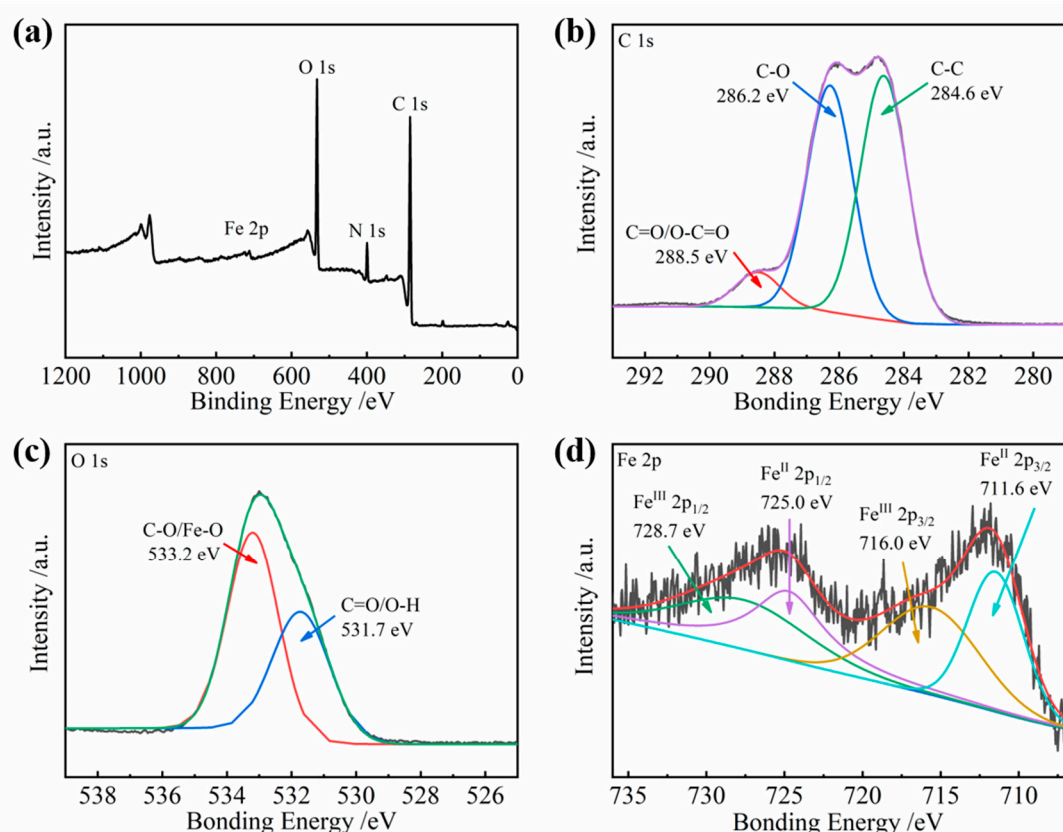
The preparation of PAN nanofibrous membranes coated with TA/Fe<sup>III</sup> complexes was accomplished according to the strategy depicted in Scheme 1. The abundant phenolic hydroxyl groups of TA not only make it easy to adhere to the surface of fibers but also can combine with Fe<sup>III</sup> to form the complexes through strongly metal chelation [22,24]. Therefore, during the layer-by-layer deposition process, TA molecules diffused into the surfaces of nanofibers as the PAN membrane was soaked into the TA solution. Subsequently, Fe<sup>III</sup> cations rapidly reacted with TA molecules to form the TA/Fe<sup>III</sup> complexes coating on the surface of PAN nanofibrous membranes. The coating process was repeated until the desired modified PAN nanofibrous membranes are obtained. As observed in Figure 1, the intensity of PAN characteristic bands at 2937 cm<sup>-1</sup> and 2242 cm<sup>-1</sup>, which correspond to the asymmetrical bending of C–H and the stretching vibration of C≡N, respectively [25], decreased obviously with the number of coating cycles. In the meanwhile, the typical adsorption bands of TA appeared in the IR spectra of modified PAN nanofibrous membranes. These bands, at 1712 cm<sup>-1</sup>, 1320 cm<sup>-1</sup>, 1201 cm<sup>-1</sup> and 757 cm<sup>-1</sup>, were assigned to the C=O stretching vibration of carbonyl groups, the –OH in-plane bending vibration of phenolic hydroxyl groups, the C–O stretching band of phenolic hydroxyl groups, and the C–H bending vibration of aromatic rings, respectively [26,27]. Moreover, because of the metal chelation between TA and Fe<sup>III</sup>, the –OH in-plane bend of TA shifted from 1320 to the higher wavenumber in the spectra of modified PAN nanofibrous membranes. The intensity and the location changes of characteristic bands confirmed the successful deposition of TA and Fe<sup>III</sup> and the formation of TA/Fe<sup>III</sup> complexes on the surface of membranes. Furthermore, the quantity of TA/Fe<sup>III</sup> complexes presented an increasing trend with the number of coating cycles.



**Figure 1.** FTIR-ATR spectra of PAN, PAN/(TA/Fe<sup>III</sup>)<sub>1</sub>, PAN/(TA/Fe<sup>III</sup>)<sub>3</sub>, PAN/(TA/Fe<sup>III</sup>)<sub>5</sub>, PAN/(TA/Fe<sup>III</sup>)<sub>7</sub> nanofibrous membranes.

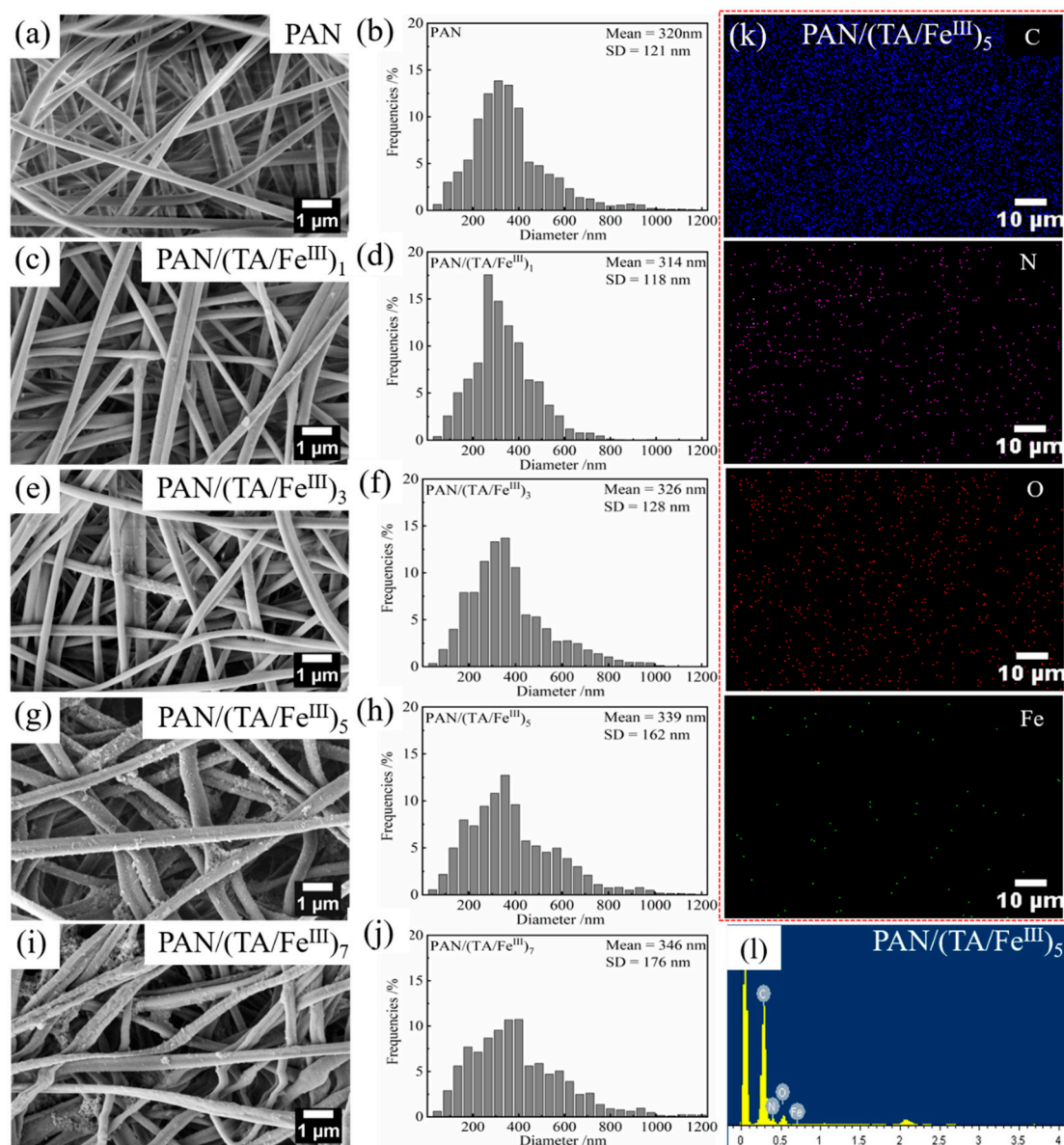
In order to further confirm the surface chemical compositions of membranes, XPS analysis is performed in Figure 2. In the full survey XPS of PAN/(TA/Fe<sup>III</sup>)<sub>5</sub> nanofibrous membrane (Figure 2a), characteristic peaks assigned to C 1s, O 1s, N 1s, and Fe 2p can be clearly observed, indicating the existence of TA and Fe<sup>III</sup> components. The high resolution

C 1s spectrum (Figure 2b) showed three dominant peaks at 284.6 eV, 286.2 eV, and 288.5 eV, assigned to C–C/C=C, C–O, and C=O/O–C=O bonds, respectively [28]. Deconvolution of O 1s spectrum (Figure 2c) displayed two peaks at 531.7 eV and 533.2 eV, corresponding to C–O/Fe–O, and C=O/O–H, which possibly pertained to the chelating structure of the TA/Fe<sup>III</sup> complexes [12,29,30]. In the Fe 2p spectrum (Figure 2d), the peaks at 711.6 eV and 725.0 eV were assigned separately to Fe 2p<sub>3/2</sub> and Fe 2p<sub>1/2</sub> of Fe<sup>II</sup>, while the peaks at 716.0 eV and 728.7 eV were attributed to Fe 2p<sub>3/2</sub> and Fe 2p<sub>1/2</sub> of Fe<sup>III</sup>, respectively [31,32]. Two valence states of Fe element showed that TA could reduce partial Fe<sup>III</sup> cations to the lower state during the self-assembly of TA/Fe<sup>III</sup> complexes [33].



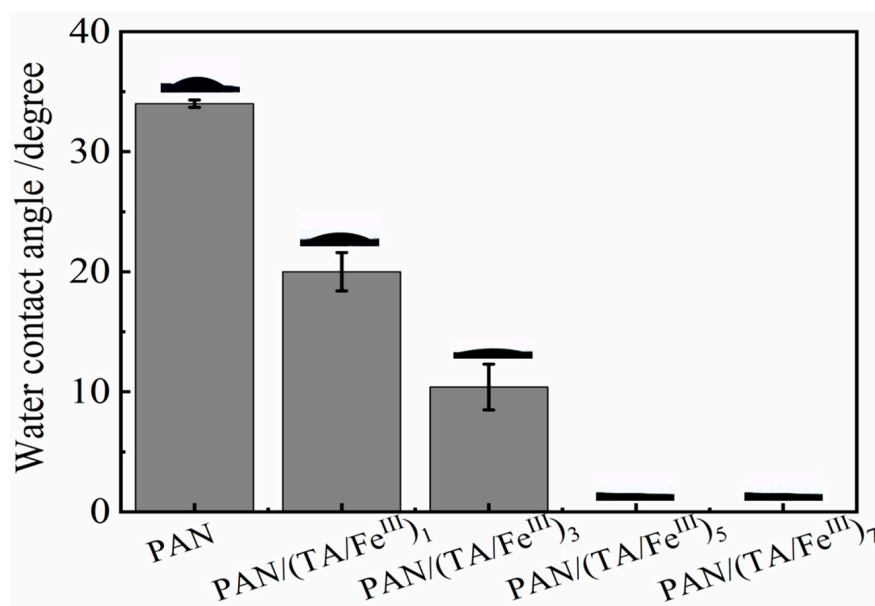
**Figure 2.** XPS (a), C1s (b), O1s (c) and Fe 2p (d) spectra of PAN/(TA/Fe<sup>III</sup>)<sub>5</sub> nanofibrous membrane.

Figure 3 presents the morphology of PAN nanofibrous membranes before and after the deposition of TA and Fe<sup>III</sup>. The bare PAN nanofibrous membrane consisted of smooth and random nanofibers with a mean diameter of about 320 nm. After layer-by-layer deposition of TA and Fe<sup>III</sup>, small grains can be seen on the surface of nanofibers. Note that the number of grains increased, and grains gradually aggregated as the increase of coating cycles, resulting in the roughening nanofiber surface and the increasing nanofiber diameter. Especially after seven coating cycles, the large size of aggregations unevenly distributed in the interfibrous pores (Figure 3i). This phenomenon could be due to the strong interactions between TA and Fe<sup>III</sup>, which made subsequent TA and Fe<sup>III</sup> tend to bound the TA/Fe<sup>III</sup> complexes that had already adhered on the surface of nanofibers, rather than continue to uniformly deposit on the surface of nanofibers [34]. In addition, the distribution of the elements in Figure 3k, l also supported that the modified PAN nanofibrous membranes contained TA and Fe<sup>III</sup>, which is consistent with the above analysis.



**Figure 3.** SEM images and fiber diameter distribution histograms of PAN (a,b), PAN/(TA/Fe<sup>III</sup>)<sub>1</sub> (c,d), PAN/(TA/Fe<sup>III</sup>)<sub>3</sub> (e,f), PAN/(TA/Fe<sup>III</sup>)<sub>5</sub> (g,h), and PAN/(TA/Fe<sup>III</sup>)<sub>7</sub> (i,j) nanofibrous membranes. Elemental mapping of C, N, O and Fe (k) and EDS (l) of the PAN/(TA/Fe<sup>III</sup>)<sub>5</sub> nanofibrous membrane.

The hydrophilic properties of PAN nanofibrous membranes coated with TA/Fe<sup>III</sup> complexes are investigated in Figure 4. The water contact angle of the bare PAN nanofibrous membrane was about 35°, revealing the hydrophilicity of PAN. After being coated with TA/Fe<sup>III</sup> complexes, the modified PAN nanofibrous membranes showed smaller water contact angles. When the number of coating cycles was more than five, the water droplet dissolved immediately once contacting with the modified PAN nanofibrous membranes, illustrating that the membranes became more and more hydrophilic. The changes of water contact angles indicated that the TA/Fe<sup>III</sup> complexes can enhance the hydrophilicity of PAN membranes, which can be attributed to the hydrophilic groups of TA. On the other hand, it also confirmed that more TA/Fe<sup>III</sup> complexes adhered on the PAN nanofibrous membranes with an increase of coating cycle.



**Figure 4.** Water contact angles of PAN, PAN/(TA/Fe<sup>III</sup>)<sub>1</sub>, PAN/(TA/Fe<sup>III</sup>)<sub>3</sub>, PAN/(TA/Fe<sup>III</sup>)<sub>5</sub>, PAN/(TA/Fe<sup>III</sup>)<sub>7</sub> nanofibrous membranes.

### 3.2. Photocatalytic Activity

Rhodamine B (RhB), one of the most important cationic xanthene dyes, has been widely applied in the textile industry [35]. Due to its high stability, non-biodegradability, and toxicity, the discharge of dyeing wastewater containing RhB into the water bodies seriously endangers human health and the ecological environment. Herein, RhB was chosen as a model pollutant to evaluate the photocatalytic activities of TA/Fe<sup>III</sup> complexes modified PAN nanofibrous membranes shown in Figure 5. Before the photodegradation experiment, a dark adsorption test was carried out, in which the photocatalyst fully contacted the target pollutant in the dark for 1 h to the establishment of the adsorption–desorption equilibrium. As shown in Figure 5a, the amount of adsorbed RhB by modified PAN nanofibrous membranes was much higher than that by the bare PAN nanofibrous membrane, owing to the contribution of TA/Fe<sup>III</sup> complexes. The stronger adsorption affinity is beneficial for photocatalyst to the subsequent photocatalytic degradation process. As the photodegradation experiment was performed under light illumination, it can be seen that RhB could be hardly degraded by the bare PAN nanofibrous membrane. In comparison, RhB was almost completely degraded by PAN/(TA/Fe<sup>III</sup>)<sub>1</sub>, PAN/(TA/Fe<sup>III</sup>)<sub>3</sub>, and PAN/(TA/Fe<sup>III</sup>)<sub>5</sub> nanofibrous membranes after 360 min illumination (Figure 5b). It fully demonstrated the photocatalysis of TA/Fe<sup>III</sup> complexes. Furthermore, among these modified PAN nanofibrous membranes, the photocatalytic activity was enhanced with the number of coating cycles. The final degradation efficiency of PAN/(TA/Fe<sup>III</sup>)<sub>5</sub> nanofibrous membrane reached to 98% after 360 min illumination (Figure 5d). And the degradation efficiency of PAN/(TA/Fe<sup>III</sup>)<sub>1</sub> and PAN/(TA/Fe<sup>III</sup>)<sub>3</sub> nanofibrous membranes both exceeded 90%. It means that the loaded amount of TA/Fe<sup>III</sup> complexes contributed to the improvement of the observed photocatalytic behavior. However, when the number of coating cycles exceed 5, the photocatalytic activity of the membrane was found to decrease, and the final degradation efficiency was only 72%. The reason may be that the aggregation of TA/Fe<sup>III</sup> complexes shown in Figure 3i can reduce the number of active sites, thus reducing the photocatalytic efficiency [36]. In addition, Figure 5c also revealed that PAN/(TA/Fe<sup>III</sup>)<sub>5</sub> nanofibrous membrane exhibited an excellent photocatalytic activity with a much higher kinetic constant based on the fitting to kinetic pseudo-first-order model.

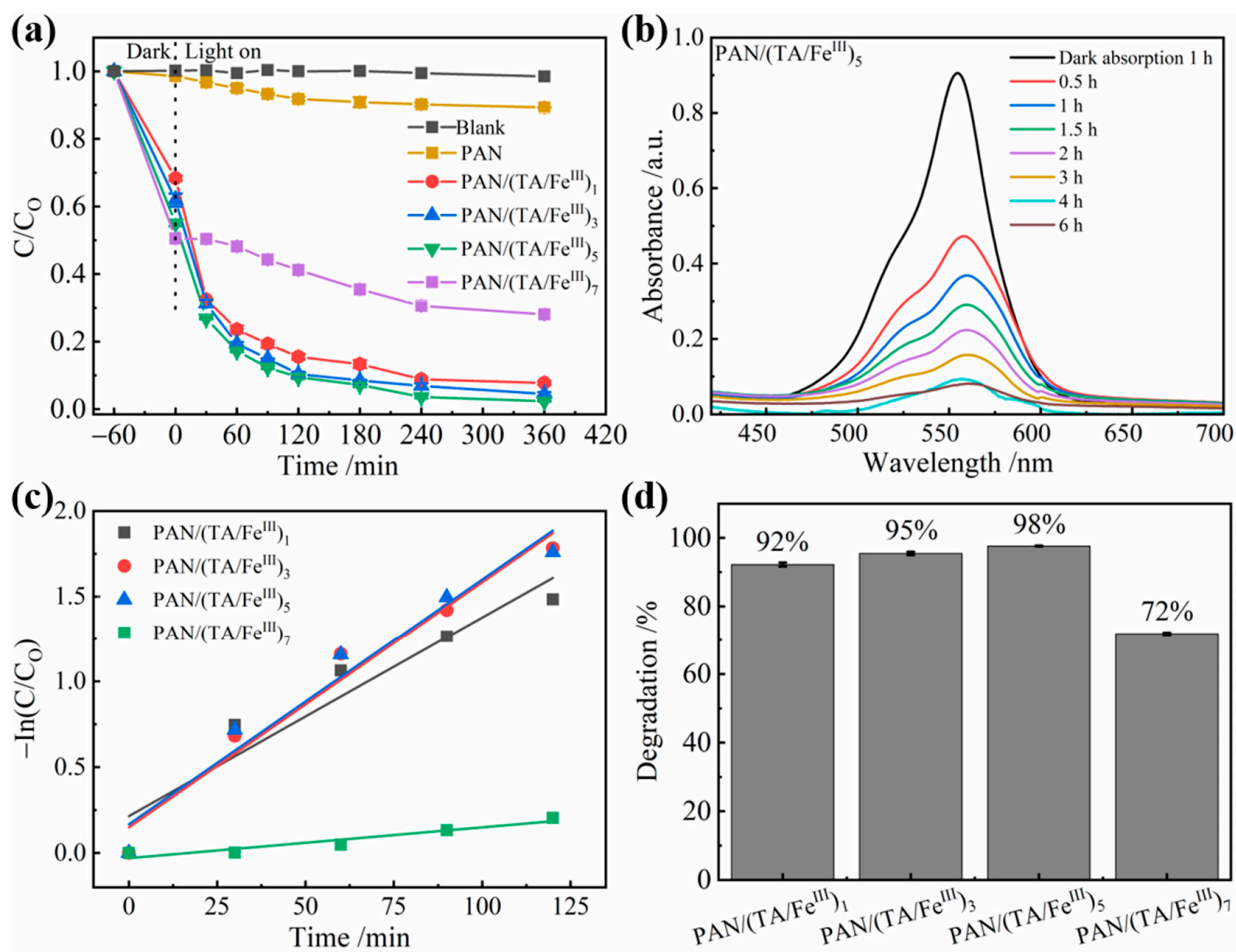


**Figure 5.** Photocatalytic degradation efficiency (a), UV-vis absorbance spectra of RhB (b), linear simulation curves of the RhB photodegradation (c), and degradation efficiency of RhB after 360 min illumination (d) over PAN/(TA/Fe<sup>III</sup>)<sub>1</sub>, PAN/(TA/Fe<sup>III</sup>)<sub>3</sub>, PAN/(TA/Fe<sup>III</sup>)<sub>5</sub>, and PAN/(TA/Fe<sup>III</sup>)<sub>7</sub> nanofibrous membranes.

### 3.3. Light Absorbance Capability

To understand the role of TA/Fe<sup>III</sup> complexes during the photocatalytic process, the optical properties of modified PAN nanofibrous membranes were investigated in depth. Figure 6 gives the UV-vis-NIR spectra of the bare PAN nanofibrous membranes and PAN nanofibrous membranes coated with TA/Fe<sup>III</sup> complexes. Compared with the bare PAN nanofibrous membrane, the light absorbance intensities of modified PAN nanofibrous membranes were enhanced obviously in the 400–1000 nm range. The increased light absorbance capabilities were attributed to the d-d transitions and the ligand-to-metal charge transfer (LMCT) in the TA/Fe<sup>III</sup> complexes [37]. With the increase of coating cycles, more TA/Fe<sup>III</sup> complexes coated on the PAN membranes, leading to the stronger light harvesting capabilities. Whereas, the aggregation of TA/Fe<sup>III</sup> complexes in the PAN/(TA/Fe<sup>III</sup>)<sub>7</sub> nanofibrous membrane may interfere with the active centers to receive the light radiation. The stronger light absorbance capability contributed to generating more free radicals for the photodegradation of RhB [12,38].

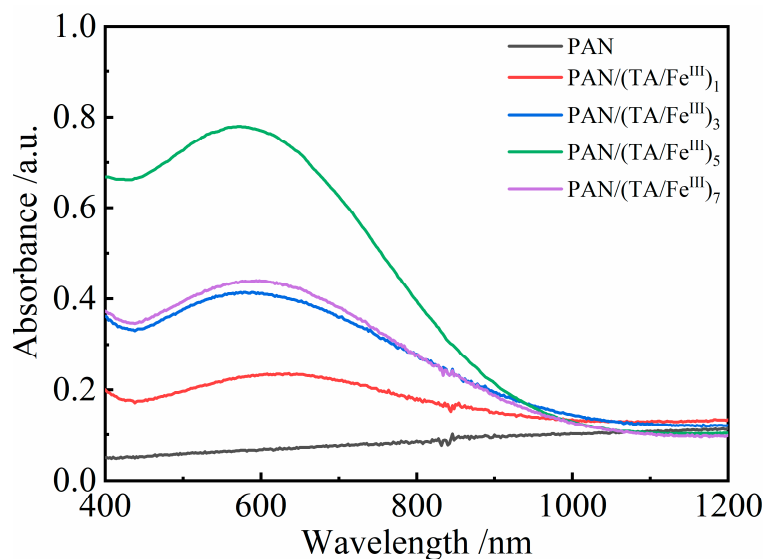


**Figure 6.** UV-vis-NIR spectra of PAN, PAN/(TA/Fe<sup>III</sup>)<sub>1</sub>, PAN/(TA/Fe<sup>III</sup>)<sub>3</sub>, PAN/(TA/Fe<sup>III</sup>)<sub>5</sub>, PAN/(TA/Fe<sup>III</sup>)<sub>7</sub> nanofibrous membranes.

### 3.4. Stability of Photocatalyst

The stability of the photocatalyst was evaluated by the cycling tests shown in Figure 7a. Although the photocatalytic performance decreased slightly after each photocatalytic cycle, the degradation efficiency remained above 70%. To analyze the reason for the change in the photocatalytic property, the morphology of the PAN/(TA/Fe<sup>III</sup>)<sub>5</sub> nanofibrous membrane after the cycling tests was investigated in Figure 7c. Compared to the original morphology of the membrane, there were only a few grains fixed on the surface of the membrane after the cycling tests. It revealed that the adhesive force between TA/Fe<sup>III</sup> complexes and PAN nanofibrous membrane should be further improved. Nevertheless, the above results confirmed the PAN nanofibrous membrane coated with TA/Fe<sup>III</sup> complexes displayed high photocatalytic performance and reusability.

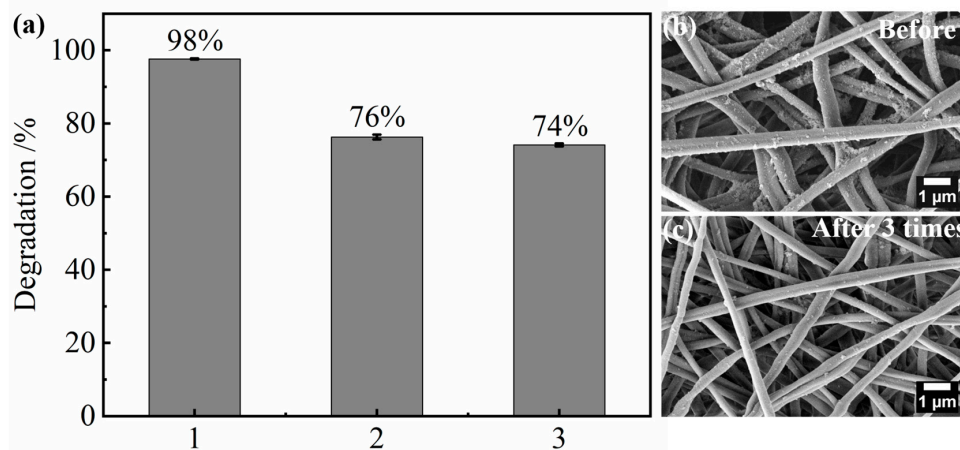


**Figure 7.** Degradation efficiency of RhB after 360 min illumination (a) and SEM images over the PAN/(TA/Fe<sup>III</sup>)<sub>5</sub> nanofibrous membrane before (b) and after (c) recycling.

## 4. Conclusions

In this work, the PAN nanofibrous membrane coated with TA/Fe<sup>III</sup> complexes was fabricated by layer-by-layer deposition of TA and Fe<sup>III</sup> cations for efficient photocatalysis. The analysis of chemical structure, morphology and hydrophilicity confirmed the successful self-assembly of TA/Fe<sup>III</sup> complexes on the surface of PAN nanofibrous membranes. Furthermore, the amount and morphology of TA/Fe<sup>III</sup> complexes in the PAN nanofibrous

membranes can be adjusted based on the coating cycles. More importantly, the modified PAN nanofibrous membranes showed excellent photocatalytic activities owing to their great light absorption capabilities. Therefore, the PAN nanofibrous membrane coated with TA/Fe<sup>III</sup> complexes could be used as a novel photocatalyst with high efficiency and reusability for dyeing wastewater treatment.

**Supplementary Materials:** The following supporting information can be downloaded at: <https://www.mdpi.com/article/10.3390/coatings13071212/s1>, Figure S1: The standard curve titration diagram of RhB solution.

**Author Contributions:** Conceptualization, X.C.; methodology, X.C. and J.M.; formal analysis, X.C.; investigation, L.Z.; resources, X.C., F.Z. and J.L.; writing—original draft preparation, X.C.; writing—review and editing, J.L.; funding acquisition, X.C., T.P. and J.L. All authors have read and agreed to the published version of the manuscript.

**Funding:** This research received no external funding.

**Institutional Review Board Statement:** No applicable.

**Informed Consent Statement:** No applicable.

**Data Availability Statement:** The data presented in this study are available on request from the corresponding author.

**Acknowledgments:** This study was financially supported by the Science Foundation of Zhejiang Sci-Tech University (21202240-Y). Meanwhile, this work was also funded by Zhejiang Provincial Natural Science Foundation of China under Grant No. LGG22E030008.

**Conflicts of Interest:** The authors declare no conflict of interest.

## References

1. Ito, T.; Adachi, Y.; Yamanashi, Y.; Shimada, Y. Long-term natural remediation process in textile dye-polluted river sediment driven by bacterial community changes. *Water Res.* **2016**, *100*, 458–465. [[CrossRef](#)] [[PubMed](#)]
2. Carneiro, P.A.; Umbuzeiro, G.A.; Oliveira, D.P.; Zanoni, M.V.B. Assessment of water contamination caused by a mutagenic textile effluent/dyehouse effluent bearing disperse dyes. *J. Hazard. Mater.* **2010**, *174*, 694–699. [[CrossRef](#)] [[PubMed](#)]
3. Fu, J.; Zhu, J.; Wang, Z.; Wang, Y.; Wang, S.; Yan, R.; Xu, Q. Highly-efficient and selective adsorption of anionic dyes onto hollow polymer microcapsules having a high surface-density of amino groups: Isotherms, kinetics, thermodynamics and mechanism. *J. Colloid Interface Sci.* **2019**, *542*, 123–135. [[CrossRef](#)] [[PubMed](#)]
4. Wang, T.; Wu, H.; Zhao, S.; Zhang, W.; Tahir, M.; Wang, Z.; Wang, J. Interfacial polymerized and pore-variable covalent organic framework composite membrane for dye separation. *Chem. Eng. J.* **2020**, *384*, 123347–123356. [[CrossRef](#)]
5. Hao, N.; Nie, Y.; Xu, Z.; Jin, C.; Fyda, T.J.; Zhang, J.X. Microfluidics-enabled acceleration of Fenton oxidation for degradation of organic dyes with rod-like zero-valent iron nanoassemblies. *J. Colloid Interface Sci.* **2020**, *559*, 254–262. [[CrossRef](#)]
6. Bilińska, L.; Blus, K.; Gmurek, M.; Ledakowicz, S. Coupling of electrocoagulation and ozone treatment for textile wastewater reuse. *Chem. Eng. J.* **2019**, *358*, 992–1001. [[CrossRef](#)]
7. Rafiq, A.; Ikram, M.; Ali, S.; Niaz, F.; Khan, M.; Khan, Q.; Maqbool, M. Photocatalytic degradation of dyes using semiconductor photocatalysts to clean industrial water pollution. *J. Ind. Eng. Chem.* **2021**, *97*, 111–128. [[CrossRef](#)]
8. Koe, W.S.; Lee, J.W.; Chong, W.C.; Pang, Y.L.; Sim, L.C. An overview of photocatalytic degradation: Photocatalysts, mechanisms, and development of photocatalytic membrane. *Environ. Sci. Pollut. Res.* **2020**, *27*, 2522–2565. [[CrossRef](#)]
9. Chen, D.; Cheng, Y.; Zhou, N.; Chen, P.; Wang, Y.; Li, K.; Huo, S.; Cheng, P.; Peng, P.; Zhang, R. Photocatalytic degradation of organic pollutants using TiO<sub>2</sub>-based photocatalysts: A review. *J. Clean. Prod.* **2020**, *268*, 121725–121738. [[CrossRef](#)]
10. Karthik, K.; Raghu, A.; Reddy, K.R.; Ravishankar, R.; Sangeeta, M.; Shetti, N.P.; Reddy, C.V. Green synthesis of Cu-doped ZnO nanoparticles and its application for the photocatalytic degradation of hazardous organic pollutants. *Chemosphere* **2022**, *287*, 132081–132090. [[CrossRef](#)]
11. Fu, J.; Yu, J.; Jiang, C.; Cheng, B. g-C<sub>3</sub>N<sub>4</sub>-Based heterostructured photocatalysts. *Adv. Energy Mater.* **2018**, *8*, 1701503–1701533. [[CrossRef](#)]
12. Xue, B.; Li, Q.; Wang, L.; Deng, M.; Zhou, H.; Li, N.; Tan, M.; Hao, D.; Du, H.; Wang, Q. Ferric-ellagate complex: A promising multifunctional photocatalyst. *Chemosphere* **2023**, *332*, 138829–138839. [[CrossRef](#)] [[PubMed](#)]
13. Kumar, V.; Singh, V.; Kim, K.-H.; Kwon, E.E.; Younis, S.A. Metal-organic frameworks for photocatalytic detoxification of chromium and uranium in water. *Coord. Chem. Rev.* **2021**, *447*, 214148–2151468. [[CrossRef](#)]
14. Lv, S.-W.; Liu, J.-M.; Zhao, N.; Li, C.-Y.; Wang, Z.-H.; Wang, S. A novel cobalt doped MOF-based photocatalyst with great applicability as an efficient mediator of peroxydisulfate activation for enhanced degradation of organic pollutants. *New J. Chem.* **2020**, *44*, 1245–1252. [[CrossRef](#)]

15. Liu, X.; Zhang, L.; Li, Y.; Xu, X.; Du, Y.; Jiang, Y.; Lin, K. A novel heterostructure coupling MOF-derived fluffy porous indium oxide with g-C<sub>3</sub>N<sub>4</sub> for enhanced photocatalytic activity. *Mater. Res. Bull.* **2021**, *133*, 111078–111088. [[CrossRef](#)]
16. Yan, W.; Shi, M.; Dong, C.; Liu, L.; Gao, C. Applications of tannic acid in membrane technologies: A review. *Adv. Colloid Interface Sci.* **2020**, *284*, 102267–102289. [[CrossRef](#)]
17. Cheng, Q.; He, X.; Guo, X.; He, S.; Rong, Q. Enhanced visible-light harvesting of triazine-based covalent organic frameworks by incorporating FeIII-tannic acid complexes for high-efficiency photocatalysis. *Microporous Mesoporous Mater.* **2022**, *341*, 112107–112114. [[CrossRef](#)]
18. Çakar, S.; Özacar, M. Fe–tannic acid complex dye as photo sensitizer for different morphological ZnO based DSSCs. *Spectrochim. Acta Part A* **2016**, *163*, 79–88. [[CrossRef](#)]
19. Kim, N.; Lee, I.; Choi, Y.; Ryu, J. Molecular design of heterogeneous electrocatalysts using tannic acid-derived metal–phenolic networks. *Nanoscale* **2021**, *13*, 20374–20386. [[CrossRef](#)] [[PubMed](#)]
20. Chong, G.; Su, R.; Gu, J.; Yang, Y.; Zhang, T.; Zang, J.; Zhao, Y.; Zheng, X.; Liu, Y.; Ruan, S. Catalytic nanovaccine for cancer immunotherapy: A NADPH oxidase-inspired Fe-polyphenol network nanovaccine for enhanced antigen cross-presentation. *Chem. Eng. J.* **2022**, *435*, 134993–135004. [[CrossRef](#)]
21. Pan, Y.; Qin, R.; Hou, M.; Xue, J.; Zhou, M.; Xu, L.; Zhang, Y. The interactions of polyphenols with Fe and their application in Fenton/Fenton-like reactions. *Sep. Purif. Technol.* **2022**, *300*, 121831–121847. [[CrossRef](#)]
22. Yang, L.; Han, L.; Ren, J.; Wei, H.; Jia, L. Coating process and stability of metal-polyphenol film. *Colloids Surf. A* **2015**, *484*, 197–205. [[CrossRef](#)]
23. Hotaling, N.A.; Bharti, K.; Kriel, H.; Simon, C.G., Jr. Diameter]: A validated open source nanofiber diameter measurement tool. *Biomaterials* **2015**, *61*, 327–338. [[CrossRef](#)] [[PubMed](#)]
24. Ejima, H.; Richardson, J.J.; Caruso, F. Metal-phenolic networks as a versatile platform to engineer nanomaterials and biointerfaces. *Nano Today* **2017**, *12*, 136–148. [[CrossRef](#)]
25. Lee, J.; Yoon, J.; Kim, J.H.; Lee, T.; Byun, H. Electrospun PAN–GO composite nanofibers as water purification membranes. *J. Appl. Polym. Sci.* **2018**, *135*, 45858–45866. [[CrossRef](#)]
26. Tang, S.; Chi, K.; Yong, Q.; Catchmark, J.M. Synthesis of cationic bacterial cellulose using a templated metal phenolic network for antibacterial applications. *Cellulose* **2021**, *28*, 9283–9296. [[CrossRef](#)]
27. Zhou, A.; Zhang, Y.; Zhang, X.; Deng, Y.; Huang, D.; Huang, C.; Qu, Q. Quaternized chitin/tannic acid bilayers layer-by-layer deposited poly (lactic acid)/polyurethane nanofibrous mats decorated with photoresponsive complex and silver nanoparticles for antibacterial activity. *Int. J. Biol. Macromol.* **2022**, *201*, 448–457. [[CrossRef](#)]
28. Li, Y.; Fu, R.; Duan, Z.; Zhu, C.; Fan, D. Construction of multifunctional hydrogel based on the tannic acid-metal coating decorated MoS<sub>2</sub> dual nanozyme for bacteria-infected wound healing. *Bioact. Mater.* **2022**, *9*, 461–474. [[CrossRef](#)]
29. Xu, W.; Han, E.-H.; Wang, Z. Effect of tannic acid on corrosion behavior of carbon steel in NaCl solution. *J. Mater. Sci. Technol.* **2019**, *35*, 64–75. [[CrossRef](#)]
30. Sivkov, D.V.; Petrova, O.V.; Nekipelov, S.V.; Vinogradov, A.S.; Skandakov, R.N.; Bakina, K.A.; Isaenko, S.I.; Ob’edkov, A.M.; Kaverin, B.S.; Vilkov, I.V. Quantitative Characterization of Oxygen-Containing Groups on the Surface of Carbon Materials: XPS and NEXAFS Study. *Appl. Sci.* **2022**, *12*, 7744. [[CrossRef](#)]
31. Yao, Y.; Yu, M.; Yin, H.; Wei, F.; Zhang, J.; Hu, H.; Wang, S. Tannic acid-Fe coordination derived Fe/N-doped carbon hybrids for catalytic oxidation processes. *Appl. Surf. Sci.* **2019**, *489*, 44–54. [[CrossRef](#)]
32. Huang, Y.; Lin, Q.; Yu, Y.; Yu, W. Functionalization of wood fibers based on immobilization of tannic acid and in situ complexation of Fe (II) ions. *Appl. Surf. Sci.* **2020**, *510*, 145436–145443. [[CrossRef](#)]
33. Zhang, L.; Wan, S.-S.; Li, C.-X.; Xu, L.; Cheng, H.; Zhang, X.-Z. An adenosine triphosphate-responsive autocatalytic fenton nanoparticle for tumor ablation with self-supplied H<sub>2</sub>O<sub>2</sub> and acceleration of Fe (III)/Fe (II) conversion. *Nano Lett.* **2018**, *18*, 7609–7618. [[CrossRef](#)] [[PubMed](#)]
34. Ringwald, C.; Ball, V. Layer-by-layer deposition of tannic acid and Fe<sup>3+</sup> cations is of electrostatic nature but almost ionic strength independent at pH 5. *J. Colloid Interface Sci.* **2015**, *450*, 119–126. [[CrossRef](#)]
35. Al-Gheethi, A.A.; Azhar, Q.M.; Kumar, P.S.; Yusuf, A.A.; Al-Buriahi, A.K.; Mohamed, R.M.S.R.; Al-Shaibani, M.M. Sustainable approaches for removing Rhodamine B dye using agricultural waste adsorbents: A review. *Chemosphere* **2022**, *287*, 132080–132090. [[CrossRef](#)]
36. Jian, S.; Tian, Z.; Hu, J.; Zhang, K.; Zhang, L.; Duan, G.; Yang, W.; Jiang, S. Enhanced visible light photocatalytic efficiency of La-doped ZnO nanofibers via electrospinning-calcination technology. *Adv. Powder Mater.* **2022**, *1*, 100004–100011. [[CrossRef](#)]
37. Yun, G.; Besford, Q.A.; Johnston, S.T.; Richardson, J.J.; Pan, S.; Biviano, M.; Caruso, F. Self-assembly of nano-to macroscopic metal–phenolic materials. *Chem. Mater.* **2018**, *30*, 5750–5758. [[CrossRef](#)]
38. Wang, D.; Jia, F.; Wang, H.; Chen, F.; Fang, Y.; Dong, W.; Zeng, G.; Li, X.; Yang, Q.; Yuan, X. Simultaneously efficient adsorption and photocatalytic degradation of tetracycline by Fe-based MOFs. *J. Colloid Interface Sci.* **2018**, *519*, 273–284. [[CrossRef](#)]

**Disclaimer/Publisher’s Note:** The statements, opinions and data contained in all publications are solely those of the individual author(s) and contributor(s) and not of MDPI and/or the editor(s). MDPI and/or the editor(s) disclaim responsibility for any injury to people or property resulting from any ideas, methods, instructions or products referred to in the content.